analytical chemistry

pubs.acs.org/ac Article

Nonuniform Electric Field-Enhanced In-Source Declustering in High-Pressure Photoionization/Photoionization-Induced Chemical Ionization Mass Spectrometry for Operando Catalytic Reaction Monitoring

Ningbo Wan, Jichun Jiang, Fan Hu, Ping Chen, Kaixin Zhu, Dehui Deng, Yuanyuan Xie, Chenxin Wu, Lei Hua,* and Haiyang Li*

Cite This: *Anal. Chem.* 2021, 93, 2207−2214 Read Online

ACCESS | Metrics & More | Article Recommendations | Supporting Information

ABSTRACT: Photoionization mass spectrometry (PI-MS) is a powerful and highly sensitive analytical technique for online monitoring of volatile organic compounds (VOCs). However, due to the large difference of PI cross sections for different compounds and the limitation of photon energy, the ability of lamp-based PI-MS for detection of compounds with low PI cross sections and high ionization energies (IEs) is insufficient. Although the ion production rate can be improved by elevating the ion source pressure, the problem of generating plenty of cluster ions, such as $[MH]^+\cdot(H_2O)_n$ (n = 1 and 2) and $[M_2]^+$, needs be solved. In this work, we developed a new nonuniform electric field high-pressure photoionization/photoionization-induced chemical ionization (NEF-HPPI/PICI) source with the abilities of both HPPI and PICI, which was accomplished through ion−molecule reactions with high-intensity H_3O^+ reactant ions generated by photoelectron ionization (PEI) of water molecules. By establishing a nonuniform electric field in a three-zone ionization region to enhance in-source declustering and using 99.999% helium as the carrier gas, not only the formation of cluster ions was significantly diminished, but the ion transmission efficiency was also improved. Consequently, the main characteristic ion for each analyte both in HPPI and PICI occupied more than 80%, especially $[HCOOH\cdot H]^+$ with a yield ratio of 99.2% for formic acid. The analytical capacity of this system was demonstrated by operando monitoring the hydrocarbons and oxygenated VOC products during the methanol-to-olefins and methane conversion catalytic reaction processes, exhibiting wide potential applications in process monitoring, reaction mechanism research, and online quality control.

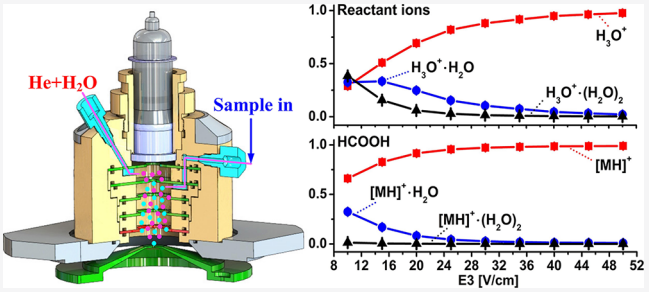

Photon ionization mass spectrometry (PI-MS) is a powerful and highly sensitive technique for online and real-time trace gas analysis of volatile organic compounds (VOCs). The applications of PI-MS have been found in various fields, such as real-time process monitoring,[1−5] environment research,[6,7] food science,[8,9] and breath analysis[10−12] during the past few decades. The photon energies of the commonly used vacuum ultraviolet krypton (VUV-Kr) discharge lamp in PI-MS are 10.0 and 10.6 eV, which are just a little higher than or equal to the ionization energies (IEs) of most VOCs,[13] leading to a high yield of molecular ions and very limited degree of fragmentation.[14] The rather soft ionization process is advantageous for online and direct MS analysis of complex mixtures owing to the easily interpreted mass spectra without excessive overlap of fragment peaks.

The ion production rate R_{PI} (ions/s) of any compound produced in a PI process is proportional to the PI cross section σ_{PI} of the molecule, the photon energy, and light intensity of the VUV light source.[10] The σ_{PI} is a measure of the probability of the ionization process for a certain photon energy and is usually measured in megabarn (Mb), whereby 1 Mb equals 10^{-18} cm^2. The σ_{PI} value of VOCs of different classes varies largely, which differs by more than 2 orders of magnitude.[15] Unsaturated hydrocarbons usually exhibit relatively larger σ_{PI}, such as 22 Mb for benzene and 24 Mb for propyne at a photon energy of 10.49 eV. Meanwhile, the σ_{PI} values are rather small for some oxygenated VOCs (OVOCs), especially for those lower-mass molecules, such as 5 Mb for propanol at a photon energy of 10.49 eV and no more than 0.2 Mb for methanol when the photon energy is less than 10.8 eV.[16] Thus, the ionization efficiency and detection sensitivity of these

Received: September 28, 2020
Accepted: December 17, 2020
Published: January 7, 2021

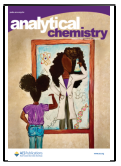

https://dx.doi.org/10.1021/acs.analchem.0c04081
Anal. Chem. 2021, 93, 2207−2214

compounds by PI-MS were not satisfactory. In addition, analytes with IEs higher than the photon energy (10.6 eV for a Kr lamp), e.g., methanol (IE = 10.84 eV) and formic acid (IE = 11.33 eV),[17] could not be effectively ionized and detected, which obviously limits the practical application of PI-MS.

Efforts have been taken to develop novel PI sources to improve the ability of PI-MS for detection of compounds with low σ_{PI} and high IEs. Zimmermann et al.[18,19] have designed a combined ion source by coupling a conventional 70 eV electron ionization (EI) module to a single-photon ionization (SPI) source in which both SPI and EI mass spectra of the analytes were obtained, and analyte molecules with IEs higher than the photon energy could be effectively ionized and detected through 70 eV EI. However, the ion source pressure must be kept low enough (below 10^{-2} Pa) to protect the heated filament, which resulted in low molecular density of analytes in the ionization region and consequently limited further improvement of the sensitivity. Zenobi et al.[20] and Li et al.[12,21,22] presented a photoelectron ionization (PEI) source based on a VUV-Kr lamp. VUV light-induced photoelectron emission was used as an alternative source of electrons for EI without the limitations of a heated filament. The PEI source could work at relatively high pressure.

Increasing the number density of analyte molecules in the ionization region by elevating the ion source pressure is a feasible way to effectively increase the ion production rate and detection sensitivity. Li and co-workers[10] have developed a high-pressure photon ionization (HPPI) source for time-of-flight mass spectrometry (TOFMS). By elevating the ion source pressure to about 700 Pa and employing a radio frequency (RF)-only quadrupole as the ion guide system, the limits of detection (LODs) down to lower-ppbv (parts per billion by volume) for some OVOCs, e.g., acetone and isoprene, were achieved. As the elevation of ion source pressure, ion−molecule reactions occur in the ion source, which can be used as another channel for ionization of analyte molecules. Li et al. developed a photoionization-generated dibromomethane cation chemical ionization (PDCI) source with an ion source pressure of 500 Pa, which utilized $CH_2Br_2^+$ as the reactant ions generated by using a VUV-Kr lamp to achieve efficient ionization of volatile sulfur compounds (VSCs) with high IEs.[6] In 2018, they used PEI to generate plenty of O_2^+ ions as the reactant ion for chemical ionization (CI) at kPa. Small *n*-alkanes with IEs higher than 10.6 eV could be effectively ionized by O_2^+ and directly detected at the sub-ppbv level.[12] For OVOCs, the proton affinities (PAs) are much higher compared with those of unsaturated hydrocarbons. Thus, the proton transfer reaction (PTR) based on the H_3O^+ (PA = 691 kJ/mol)[17] reactant ion is suitable for efficient ionization of OVOCs.[23−25] Shu et al.[11,26−29] reported a VUV-excited and CH_2Cl_2/H_2O-amplified ionization process by introducing a gas mixture of CH_2Cl_2/H_2O into the VUV ion source to generate large amounts of H_3O^+ ions. Then, the PTR between the H_3O^+ reactant ions and analyte molecules occurred to produce analyte ions $[MH]^+$ and $[MH]^+\cdot H_2O$ with the ion source pressure in the range of 500−1300 Pa. The signal intensities of some OVOCs in the PTR could be amplified by more than 3 orders of magnitude in contrast to those obtained with VUV-PI alone.

However, as the elevation of ion source pressure for higher sensitivity, cluster ions formed by ion−molecule reactions both in the HPPI and CI sources were inevitable, such as $[MH]^+\cdot(H_2O)_n$ (n = 1 and 2) and $[M_2]^+$, especially the formation of hydrated cluster ions $H_3O^+\cdot(H_2O)_n$ (n = 1 and 2) when dealing with high-humidity samples.[11,23,27] This will not only increase the complexity of the mass spectra but also affect the detection sensitivity of the analytes as the reaction capacities for the reactions of $H_3O^+\cdot(H_2O)_n$ (n = 0−2) with analyte molecules decreased as the number of water molecules (n) increased. Bohme et al.[30] studied the gas-phase kinetics of reactions with $H_3O^+\cdot(H_2O)_n$ (n = 0−2) by the flowing afterglow experiments at 300 K, which indicated that the rate coefficients for the reactions of HCOOH (for example) with H_3O^+, $H_3O^+\cdot H_2O$, and $H_3O^+\cdot(H_2O)_2$ were 2.7 ± 0.8, 2.4 ± 0.7, and 1.5 ± 0.5 (10^{-9} cm^3 $molecule^{-1}$ s^{-1}), respectively. Collision-induced dissociation (CID) of a cluster ion with neutral molecules by increasing the kinetic energy of the ion is a direct and effective method to get its core ion. In HPPI-MS, efforts have been taken to realize in-source CID to dissociate some cluster ions by elevating the ion source voltage to form a high-intensity uniform electric field throughout the ionization region.[31−33] In PTR-MS, the degree of cluster ion formation was usually regulated by choosing an appropriate value of E/N,[34,35] where E was the electric field intensity in the drift tube and N was the density of gas molecules in the drift tube. However, a higher value of E/N led to a reduced ion−molecule reaction time, which could decrease the sensitivity of PTR-MS. Additionally, the ion transmission efficiency might degrade under excessive intensity of the uniform electric field. Even so, in the analysis of high-humidity samples,[10,36,37] such as exhaled breath,[10] cluster ions $[MH]^+\cdot(H_2O)_n$ (n = 1 and 2) still existed in the mass spectra at relatively high values of the electric field intensity.

In this study, a nonuniform electric field high-pressure photoionization/photoionization-induced chemical ionization (NEF-HPPI/PICI) source with both HPPI and PICI capabilities was developed for the TOFMS. HPPI was achieved by using a VUV-Kr lamp, while PICI was accomplished through ion−molecule reactions with high-intensity H_3O^+ reactant ions generated by PEI of water molecules. To eliminate the effect of cluster ions, a nonuniform electric field in a three-zone ion source was designed. The electric field intensities of three zones as well as the type of carrier gas were investigated. The performance of this NEF-HPPI/PICI source in terms of declustering and ion beam focusing was also evaluated. Finally, applications have been demonstrated by operando monitoring the products during methane conversion and methanol-to-olefins catalytic reaction processes.

EXPERIMENTAL SECTION

VUV-Lamp-Based NEF-HPPI/PICI Source. The NEF-HPPI/PICI source was composed of a VUV lamp and a three-zone ionization region, as shown in Figure 1. A 10.6 eV VUV-Kr lamp (PKS106, Cathodeon Ltd., Cambridge, U.K.) with a photon flux of about 1×10^{12} photons/s was installed on the top of the ionization region, which consisted of six concentric stainless steel electrodes (SE1−SE6): a photoelectron acceleration electrode (SE1: 6 mm i.d., 1 mm thick), a photoelectron emission electrode (SE2: 3 mm i.d., 1 mm thick), two identical transmission electrodes (SE3 and SE4: 12 mm i.d., 1 mm thick), an ion dissociation and focusing electrode (SE5: 12 mm i.d., 1 mm thick), and a Skimmer electrode (SE6: 1 mm i.d., 4 mm thick). Four 5 mm-thick polyether−ether−ketone (PEEK) insulation annular washers (16 mm i.d.) were used to separate the electrodes, except the space between the SE5 and SE6 electrodes for excess neutral

https://dx.doi.org/10.1021/acs.analchem.0c04081
Anal. Chem. 2021, 93, 2207−2214

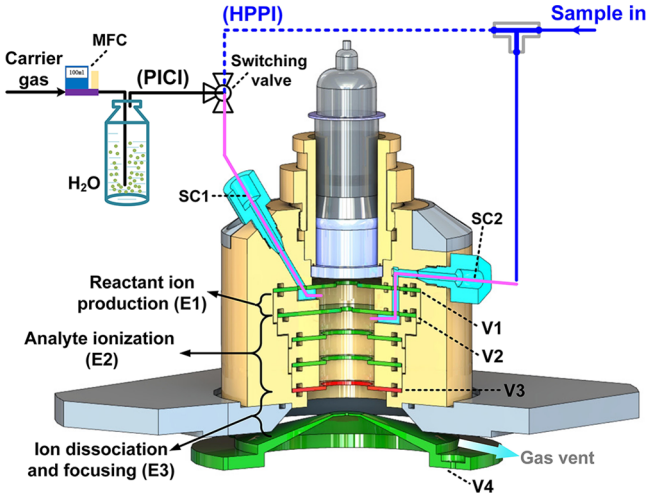

Figure 1. Cutaway diagram of the VUV-lamp-based nonuniform electric field high-pressure photoionization/photoionization-induced chemical ionization (NEF-HPPI/PICI) source (black line: PICI mode; blue line: HPPI mode; MFC: mass flow controller).

exhaust. The SE2 and SE5 electrodes partitioned the ionization region into three zones: a reactant ion production zone E1, an analyte ionization zone E2, and an ion dissociation and focusing zone E3. Gas-phase analytes and humidified helium (He) were directly introduced into the ionization region through two 250 μm i.d., 1 m long PEEK sampling capillaries (SC1 and SC2) through which the sampling flow rate was about 11 mL/min for each capillary. SC1 was used to introduce humidified He or gas-phase analytes into the reactant ion production zone, while SC2 was employed to introduce only the gas-phase analytes into the analyte ionization zone. Humidified He was obtained by bubbling of 11 mL/min high-purity He (99.999%) through purified water. The electrodes from SE2 to SE4 were electrically connected by using a 1 MΩ resistor string, and additionally, the SE5 was connected by another 1 MΩ resistor to the earth. Four positive dc voltages were individually applied to the SE1 (V1), SE2 (V2), SE5 (V3), and SE6 (V4) electrodes. The ions generated in the ionization region were transferred through the 1 mm i.d. center orifice of the Sampler electrode into a home-built radio frequency (RF)-only quadrupole TOFMS for mass analysis.

The NEF-HPPI/PICI source could work at two different operation modes, the HPPI mode and PICI mode, by simply adjusting the two dc voltages, V1 and V2, respectively, and simultaneously switching SC1 to corresponding gases. In the HPPI mode, both SC1 and SC2 were used to introduce gas-phase analytes, and the electric field intensity E1 between the SE1 and SE2 electrodes was 8 V/cm. Thus, the photoelectrons emitted from the surface of the SE2 electrode could not obtain enough energy to ionize analyte molecules, and the ionization process was dominated by PI. Meanwhile, in the PICI mode, humidified He was selected by a switching valve to flow through SC1 into the reactant ion production zone, and an electric field intensity E1 of 250 V/cm allowed the photoelectrons emitted from the surface of the SE2 electrode to get sufficiently high energy to ionize He and H_2O molecules. Plenty of H_3O^+ reactant ions were produced in the reactant ion production zone after a series of ion−molecule reactions and transferred into the analyte ionization zone to react with the analyte molecules by the PTR. The intensity of the H_3O^+ reactant ion could be regulated by adjusting the electric field intensity E1. Compared with the previously reported HPPI ion source, one of the major differences is the design of the ion dissociation and focusing zone in the NEF-HPPI/PICI source, which was employed to dissociate cluster ions and focus the ion beam by elevating the electric field intensity E3 between the SE5 and SE6 electrodes. The switching time between the two modes was less than 1 s.

RF-Only Quadrupole TOFMS. The mass spectrometer used in the experiment was a home-built RF-only quadrupole orthogonal acceleration reflectron TOFMS (see the Supporting Information, S1). A mass resolving power of 5000 (full width at half-maximum, fwhm) was achieved with a 0.5 m field-free drift tube. All the mass spectra were accumulated for 10 s at a repetition rate of 25 kHz, and all data were obtained by averaging results from six parallel measurements.

Sample Preparation. The introduction of the sample preparation method is shown in the Supporting Information, S2.

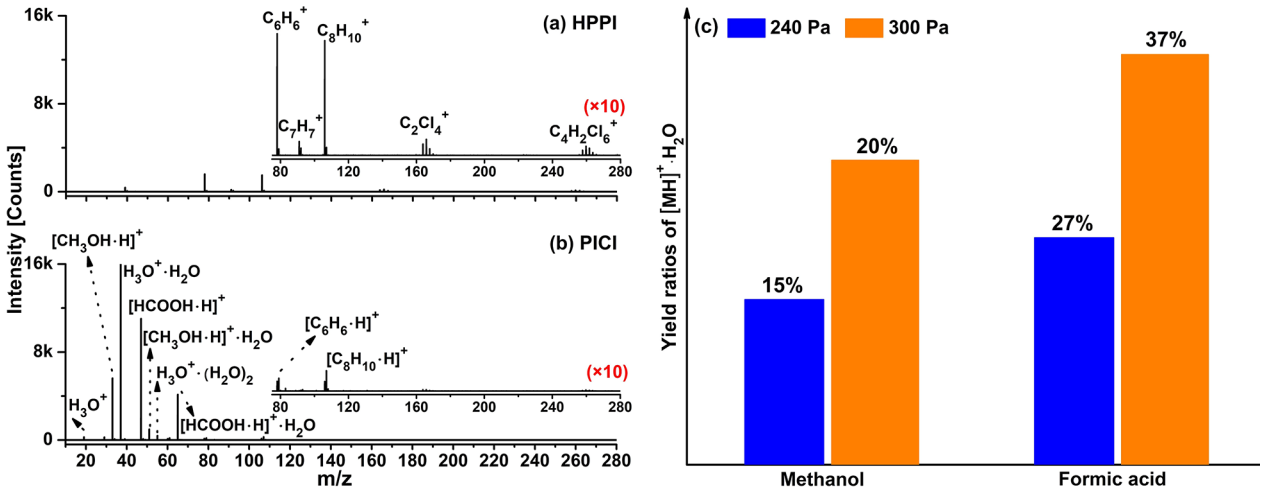

Figure 2. Mass spectra of benzene (0.5 ppmv), *p*-xylene (0.5 ppmv), tetrachloroethylene (0.5 ppmv), hexachloro-1,3-butadiene (0.5 ppmv), methanol (0.75 ppmv), and formic acid (6 ppmv) in the HPPI mode (a) and PICI mode (b), respectively. (c) Yield ratios of cluster ions $[MH]^+ \cdot H_2O$ at different ion source pressures in the PICI mode.

https://dx.doi.org/10.1021/acs.analchem.0c04081
Anal. Chem. 2021, 93, 2207−2214

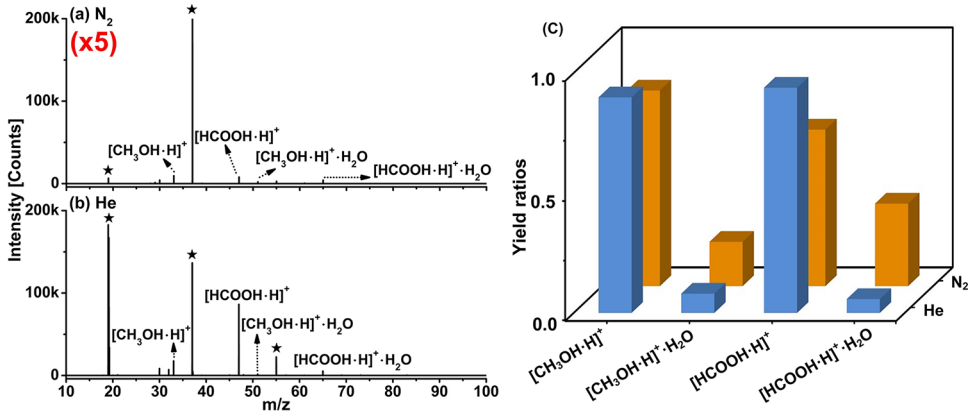

Figure 3. Mass spectra of 0.25 ppmv methanol and 5 ppmv formic acid in the carrier gas of 99.999% N_2 (a) and 99.999% He (b), respectively. (c) Yield ratios of $[MH]^+\cdot(H_2O)_n$ (n = 0 and 1) of methanol and formic acid in the carrier gas of 99.999% N_2 and 99.999% He, respectively (star: reactant ions $H_3O^+\cdot(H_2O)_n$ (n = 0, 1, and 2)).

RESULTS AND DISCUSSION

Ionization of VOCs in the HPPI and PICI Modes. Figure 2 illustrates the mass spectra of a mixed gas sample of benzene (0.5 ppmv), *p*-xylene (0.5 ppmv), tetrachloroethylene (0.5 ppmv), hexachloro-1,3-butadiene (0.5 ppmv), methanol (0.75 ppmv), and formic acid (6 ppmv) in 99.999% N_2 gas in the HPPI and PICI modes, respectively. The electric field intensities of E1, E2, and E3 were 250, 10, and 45 V/cm, respectively. The signal intensities of data with m/z greater than 75, as shown in Figure 2a,b, were magnified by 10 times. As shown in Figure 2a, only the molecular ion peaks of benzene, *p*-xylene, tetrachloroethylene, and hexachloro-1,3-butadiene appeared in the HPPI mass spectrum, besides the fragment ion peak of *p*-xylene at m/z 91 ($C_7H_7^+$). As the IEs of methanol (IE = 10.84 eV) and formic acid (IE = 11.33 eV)[17] were higher than the photon energy (10.6 eV), they were hard to be effectively ionized by HPPI (only 4 counts for methanol and 11 counts for formic acid). In the PICI mode, the OVOCs, methanol, and formic acid could be efficiently ionized by the ion−molecule reaction with the reactant ions $H_3O^+\cdot(H_2O)_n$ (n = 0, 1, and 2), producing significant mass peaks of analyte ions $[MH]^+\cdot(H_2O)_n$ (n = 0, 1, and 2) in the PICI mass spectrum. The characteristic ions for the hydrocarbons in Figure 2b are molecular ions M^+ or protonated molecular ions $[MH]^+$. However, the signal intensities of benzene, *p*-xylene, tetrachloroethylene, and hexachloro-1,3-butadiene in the PICI mode were much lower than those in the HPPI mode, which indicated that these two modes were suitable for different classes of compounds. The HPPI mode was powerful in ionization of hydrocarbons, while higher sensitivity for OVOCs can be achieved in the PICI mode. Therefore, the coupling of HPPI and PICI modes in the ion source could be a versatile ionization technique for efficient soft ionization of multiple VOC species.

A major problem for the NEF-HPPI/PICI source was that the excess hydrated cluster ions, $H_3O^+\cdot(H_2O)_n$ (n = 1 and 2) and $[MH]^+\cdot(H_2O)_n$ (n = 1 and 2), formed in the PICI mode, which not only increased the complexity of the mass spectra but also reduced the ionization efficiency of analytes with the reactant ion ($H_3O^+\cdot(H_2O)_n$ (n = 1 and 2)).[30] What is more, the degree of cluster ion formation increased as the elevation of the ion source pressure for higher sensitivity, as shown in Figure 2c. Thus, the methods for declustering by changing the carrier gas and optimizing the electric field in the ionization region were investigated in the following experiments.

Influence of Different Carrier Gases in the PICI Mode. To investigate the influence of different carrier gases on the product ion distribution in the PICI mode, the mass spectra of 0.25 ppmv methanol and 5 ppmv formic acid in the carrier gas of 99.999% N_2 and 99.999% He with the ion source pressure of both 300 Pa were acquired, respectively, as shown in Figure 3. On the one hand, there were less cluster ions formed with carrier gas He. Since the cluster formation was an exothermic reaction, more collisions between the ions and neutral molecules were required by using the lower-mass molecules (He) as the collision gas to release the excess energy from the cluster formation process.[38] In addition, the uptake of the collision energy into the N_2 internal energy might also contribute to the cluster formation in the N_2 carrier gas. Thus, the formation of cluster ions was more difficult in the He atmosphere than in N_2. On the other hand, the signal intensities of the analytes in He gas were almost 1 order of magnitude higher than those in N_2 gas. This can be attributed to the higher ion transmission efficiency in the ion source and the RF-only quadrupole region with carrier gas He, especially for the analyte ions with relatively low m/z, such as $[CH_3OH\cdot H]^+$ (m/z 33) and $[HCOOH\cdot H]^+$ (m/z 47). According to the result of an ion trajectory simulation by SIMION 8.1, the ion transmission efficiency with He gas in the ion source was about 1.5 times higher than that with N_2 gas, while more than 4 times was achieved in the RF-only quadrupole region (see the Supporting Information, S3). Therefore, high-purity He was employed as the carrier gas of the analytes in this work.

Declustering and Focusing Effect of Nonuniform Electric Field. To achieve in-source CID by elevating the electric field intensity uniformly in the whole ionization region would result in the decrease of ionization efficiency (see the Supporting Information, S4). Therefore, we made a first attempt to integrate an ion dissociation and focusing zone into the NEF-HPPI/PICI source to solve this issue. An ion trajectory calculation was carried out by SIMION 8.1 software to investigate the effect of electric field uniformity in the analyte ionization zone E2 and the ion dissociation and focusing zone E3. Five hundred ions with m/z 33 ($[CH_3OH\cdot H]^+$) and 500 ions with m/z 47 ($[HCOOH\cdot H]^+$) were defined in a circular plane (Φ = 2 mm) right below the central hole of the photoelectron emission electrode in the analyte ionization

https://dx.doi.org/10.1021/acs.analchem.0c04081
Anal. Chem. 2021, 93, 2207−2214

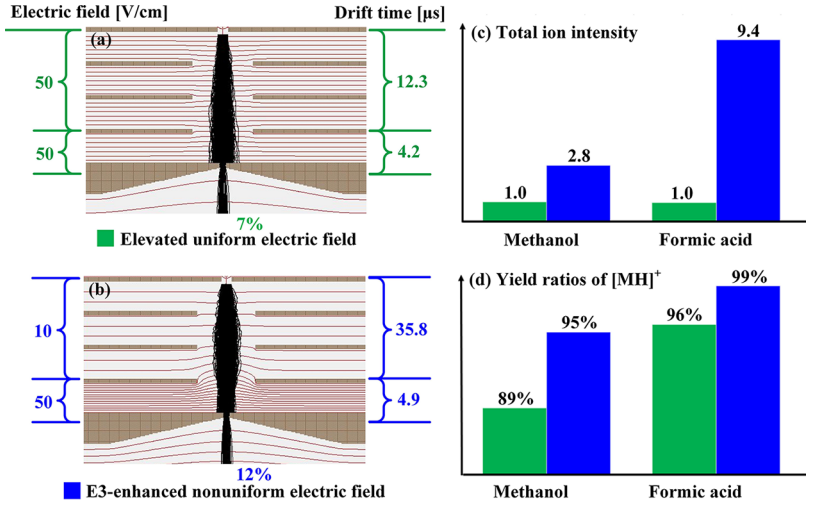

Figure 4. Ion trajectories calculated by SIMION 8.1 software in the elevated uniform electric field (a) and the E3-enhanced nonuniform electric field (b). Comparison of the total ion intensities (c) and the ratios of $[MH]^+$ (d) for methanol and formic acid in the elevated uniform electric field and E3-enhanced nonuniform electric field.

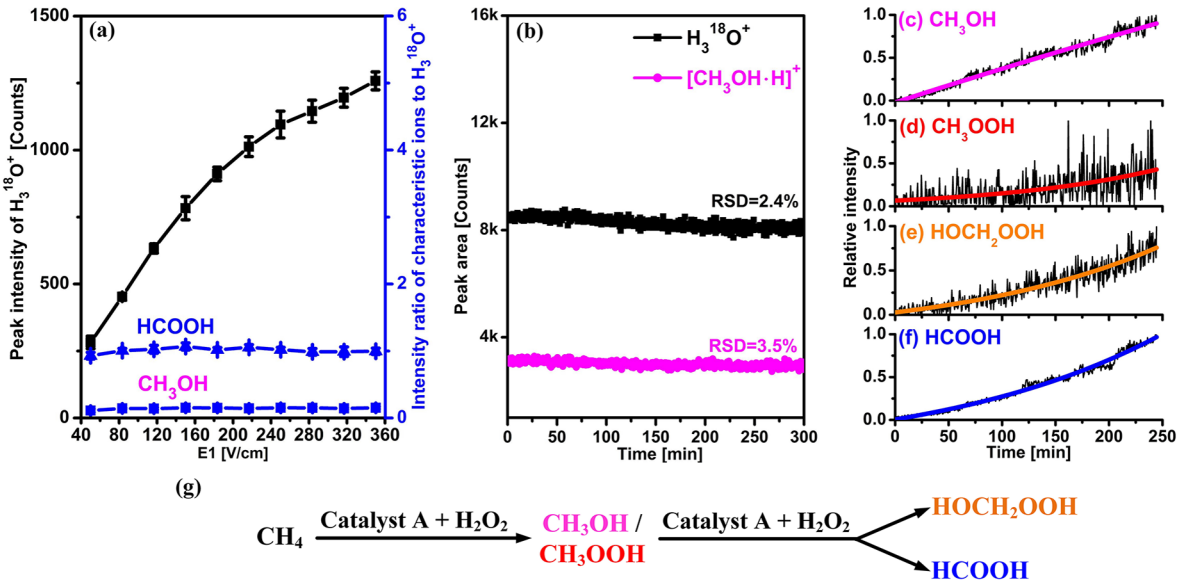

Figure 5. (a) Signal intensities of $H_3{}^{18}O^+$ reactant ions and the ratio of $[MH]^+/H_3{}^{18}O^+$ for methanol and formic acid at different electric field intensities of E1. (b) Peak area of $H_3{}^{18}O^+$ and $[CH_3OH{\cdot}H]^+$ ions as a function of monitoring time in the PICI mode. (c–f) Time course of relative intensities of four OVOC products during the methane conversion process. (g) Possible reaction path for methane oxidation.

zone. In the calculation, He was selected as the collision gas, and the ion source pressure was set at 300 Pa. Figure 4a and Figure 4b illustrate the ion trajectories and electric field distributions in the ionization zones with an elevated uniform electric field and E3-enhanced nonuniform electric field, respectively. To realize in-source CID, the electric field intensities of both E2 and E3 were elevated to 50 V/cm in the elevated uniform electric filed, while only E3 was enhanced to 50 V/cm and E2 remained at a relatively low intensity of 10 V/cm in the E3-enhanced nonuniform electric field. The drift time of ions transmitting through the E2 and E3 zones in the E3-enhanced nonuniform electrical field was about 2.5 times as long as that in the elevated uniform electrical field, which means a longer ion–molecule reaction time and higher PICI ionization efficiency in the E3-enhanced nonuniform electrical field. Furthermore, it is obvious that the ion trajectories exhibited a focusing trend in Figure 4b, and the ion transmission efficiency was calculated to be about 12% in the E3-enhanced nonuniform electrical field, which was almost 2 times as much as that in the elevated uniform electrical field (about 7%). A mixed gas sample of 0.25 ppmv methanol and 5 ppmv formic acid gas in 99.999% He was taken as an example to explore the actual difference between the configurations of the elevated uniform electric field and E3-enhanced nonuniform electric field. Similar to the calculation results by SIMION 8.1, the total ion intensities of methanol and formic acid in the E3-enhanced nonuniform electric field were 2.8 and 9.4 times as much as those in the elevated uniform electric field, respectively (Figure 4c). Although only E3 was enhanced, the degree of cluster ion formation in the E3-enhanced nonuniform electric field was even lower than that in the elevated uniform electric field, as shown in Figure 4d. More details about the influence of the electric field intensity E3 on detection sensitivity and cluster ion dissociation are shown in

https://dx.doi.org/10.1021/acs.analchem.0c04081
Anal. Chem. 2021, 93, 2207–2214

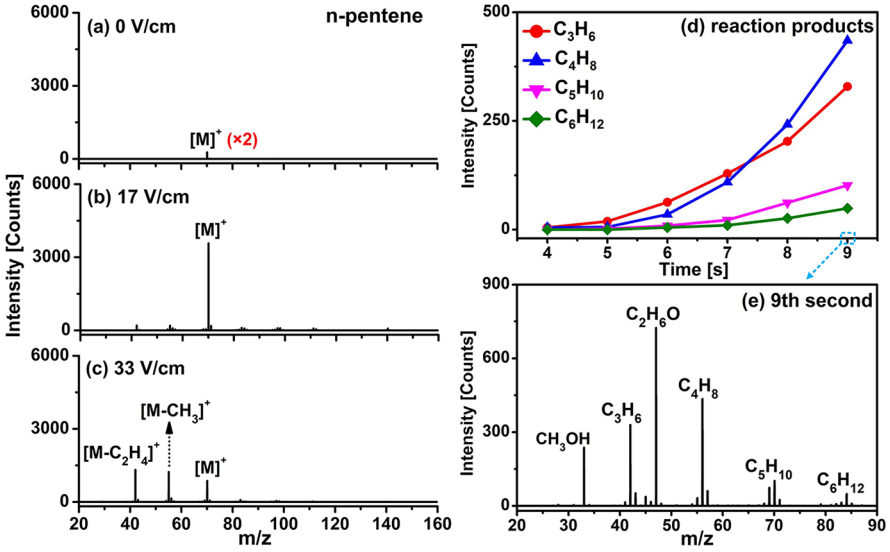

Figure 6. (a–c) Mass spectra of 890 ppm *n*-pentene at different electric field intensities of E3 in the HPPI mode. (d) Time course of reaction products in the outflow gas during the initial stage of the methanol-to-olefins reaction. (e) Mass spectrum of the light olefin products at the reaction time of the ninth second.

the Supporting Information, S5 and S6. The degree of cluster ion dissociation and the detection sensitivity can be regulated flexibly by adjusting the value of E3.

Performance of NEF-HPPI/PICI TOFMS. The analytical performance of the NEF-HPPI/PICI TOFMS for several hydrocarbons and OVOCs is summarized in the Supporting Information, S7. In the HPPI mode, the enhancement factors (ratio of response for one ionization mode over another) of HPPI over PICI toward benzene, *p*-xylene, tetrachloroethylene, and hexachloro-1,2-butadiene were determined to be 6-, 9-, 7-, and 10-fold, respectively. Meanwhile, in the PICI mode, the enhancement factors of PICI over HPPI reveal the amplification of signal intensities from 3-fold to more than 3 orders of magnitude (1885-fold) for methanol, formic acid, butanone, and diethyl ether. The LODs (S/N = 3) ranged from 0.17 to 13 ppbv (see Table S1). The linear ranges of 2–3 orders of magnitude were achieved, and the correlation coefficients were in the range of 0.9897–0.9993 (see Figure S6).

Applications on Operando Monitoring of Products in Two Microcatalytic Reaction Processes. The selective activation and orientable conversion of methane to high-value-added chemicals are a promising work and are considered the "holy grail" in catalysis. An efficient nonprecious catalyst to directly convert methane to C1 oxygenated products under mild conditions based on graphene-confined single Fe atoms has been developed in the Dalian Institute of Chemical Physics.[2] In-depth understanding of the catalytic reaction mechanism requires the information of the product variation during the reaction. Therefore, the NEF-HPPI/PICI TOFMS was used to monitor the products in operando during the reaction process.

As the VUV photon flux and the photoelectron emission efficiency of the electrode may decrease due to contamination of the window of the VUV lamp and oxidation of the electrode, especially for the analytes with relatively high concentrations, the stability will be affected during long-term measurement. As shown in Figure 5a, the black curve displays a positive correlation between the peak intensity of the $H_3{}^{18}O^+$ reactant ions (the isotope peak of $H_3{}^{16}O^+$ as the signal intensity of $H_3{}^{16}O^+$ was saturated) and the electric field intensity of E1, while the almost unchanged blue curves represent the variation trends of intensity ratios of $[MH]^+$ to $H_3{}^{18}O^+$ for 0.25 ppmv methanol and 5 ppmv formic acid as a function of the electric field intensity of E1. Obviously, the signal intensities of $[CH_3OH{\cdot}H]^+$ and $[HCOOH{\cdot}H]^+$ were proportional to those of the H_3O^+ reactant ions. Thus, it is an effective solution to improve the stability of the instrument by adjusting the electric field intensity of E1 to eliminate the fluctuation of the signal intensities of the H_3O^+ reactant ion and analyte ions in the PICI mode. Therefore, a self-adjustment algorithm was used to stabilize the intensity of the H_3O^+ reactant ions by automatically adjusting the value of E1. Figure 5b displays the peak area variations of $H_3{}^{18}O^+$ ions and $[CH_3OH{\cdot}H]^+$ ions of 0.25 ppmv methanol as a function of monitoring time after using the algorithm. As a result, the relative standard deviations (RSDs) of $H_3{}^{18}O^+$ and $[CH_3OH{\cdot}H]^+$ were only 2.4 and 3.5%, respectively.

Details of the operation conditions for the methane conversion reaction are described in the Supporting Information, S8. The OVOC products from the reaction solution carried by 99.999% He were detected in the PICI mode. The electric field intensity of E3 was elevated to a higher level (133 V/cm) in this experiment to eliminate the cluster ion $[HCOOH{\cdot}H]^+{\cdot}H_2O$ of the product HCOOH, whose peak completely coincided with the protonated ion $[HOCH_2OOH{\cdot}H]^+$ of product $HOCH_2OOH$ in the mass spectra. The catalytic reaction was continuously monitored in operando for approximately 4 h, and the results are shown in Figure 5c–f. During the reaction, the intensities of CH_3OH and CH_3OOH increased gradually over time, and the increasing rate of CH_3OH gradually decreased after 150 min, while the increasing rate of $HOCH_2OOH$ and HCOOH increased significantly in the last 90 min. This variation tendency was consistent with another similar catalyst,[2] which suggested that CH_4 was first oxidized to CH_3OH and CH_3OOH, and then, CH_3OH was further oxidized to $HOCH_2OOH$ and HCOOH.[2] The possible reaction path of methane conversion, as shown in Figure 6g, was further supported by a ^{13}C nuclear magnetic resonance (NMR)

https://dx.doi.org/10.1021/acs.analchem.0c04081
Anal. Chem. 2021, 93, 2207–2214

experiment and density functional theory (DFT) calculations in the previous work.[2]

The methanol-to-olefins reaction is of strategic significance for the production of light olefins.[39,40] In this work, the hydrocarbon products during the initial stage of the methanol-to-olefins reaction were real-time monitored in the HPPI mode with a high temporal resolution of 1 s. Details of the operation conditions for this reaction are described in the Supporting Information, S9. To investigate the influence of the electric field intensity of E3 on the ion dissociation of light olefins, 890 ppm *n*-pentene was taken as an example to optimize the electric field intensity of E3 for effectively avoiding the formation of cluster ions and suppressing the production of fragment ions. The ion source pressure was decreased to 50 Pa to further reduce the formation of olefin cluster ions, and the acquisition time of mass spectra in Figure 6a−c is 10 s. As shown in Figure 6a, when the value of E3 was initially set to 0 V/cm, only the molecular ion peak of *n*-pentene was presented in the mass spectrum without any cluster ions and fragment ions. However, the signal intensity of *n*-pentene was very weak, which was attributed to the poor ion transmission. As the electric field intensity of E3 increased to 17 V/cm (Figure 6b), the intensity of the molecular ion peak of *n*-pentene increased sharply to a maximum value with very little fragment ions and cluster ions. When the value of E3 was further elevated to 33 V/cm (Figure 6c), the molecular ion of *n*-pentene fragmented dramatically and the dominant ions were the fragments $[M\text{-}CH_3]^+$ and $[M\text{-}C_2H_4]^+$, the latter of which was identical to the molecular ion of propylene $[C_3H_6]^+$. Therefore, to avoid excessive fragments, the electric field intensity of E3 was set to 17 V/cm during the methanol-to-olefins reaction process. Figure 6d illustrates the time course of the light olefin products, propylene, butene, pentene, and hexene with a temporal resolution of 1 s during the initial stage of the methanol-to-olefins reaction, which indicates that the olefins with a higher carbon number were produced later. The mass spectrum acquired at the reaction time of the ninth second in Figure 6e shows that propylene and butene were the main products at this time, besides the reactant methanol and intermediate methyl ether.

CONCLUSIONS

It has been demonstrated that the NEF-HPPI/PICI source with a three-zone ionization region is a soft and versatile ionization technique for online MS in real-time monitoring of complex VOC mixtures. High-intensity H_3O^+ reactant ions generated by PEI of water molecules could be used to effectively ionize compounds with high IEs and low photoionization cross sections but relatively high PAs through PICI, such as OVOCs. A nonuniform electric field in the three-zone ionization region was established to enhance in-source declustering by elevating the electric field intensity of the ion dissociation and focusing zone E3 while keeping the electric field intensity in the analyte ionization zone E2 at a relatively low value. The design of the nonuniform electric field as well as the use of high-purity helium as the carrier gas not only diminished the formation of cluster ions but also improved the ion transmission efficiency. As a result, the main characteristic ion of molecule ion M^+ for HPPI and protonated molecule ion $[MH]^+$ for PICI occupied more than 80% of the total characteristic ions. The achieved LODs were down to lower-ppbv to sub-ppbv for some hydrocarbons and OVOCs. The applications on operando monitoring of two catalytic reaction processes exhibited an excellent performance and wide potential applications of the NEF-HPPI/PICI TOFMS system in process monitoring, reaction mechanism research, and online quality control.

ASSOCIATED CONTENT

Supporting Information

The Supporting Information is available free of charge at https://pubs.acs.org/doi/10.1021/acs.analchem.0c04081.

RF-only quadrupole TOFMS, sample preparation, ion transmission efficiency simulation in the ion source and RF quadrupole region with different carrier gases, influence of electric field intensities of E2 and E3 on the ion dissociation and sensitivity in the elevated uniform electric field, signal intensities of methanol and formic acid as a function of the electric field intensity E3 in the E3-enhanced nonuniform electric field, influence of the electric field intensity E3 on characteristic ion distributions, performance of the NEF-HPPI/PICI TOFMS, and operation of the methane conversion reaction and methanol-to-olefins catalytic reaction (PDF)

AUTHOR INFORMATION

Corresponding Authors

Lei Hua − *CAS Key Laboratory of Separation Science for Analytical Chemistry, Dalian Institute of Chemical Physics, Chinese Academy of Sciences, Dalian, Liaoning 116023, People's Republic of China*; Email: lhua@dicp.ac.cn; Fax: +86-411-84379517

Haiyang Li − *CAS Key Laboratory of Separation Science for Analytical Chemistry, Dalian Institute of Chemical Physics, Chinese Academy of Sciences, Dalian, Liaoning 116023, People's Republic of China*; orcid.org/0000-0002-6658-4745; Email: hli@dicp.ac.cn

Authors

Ningbo Wan − *CAS Key Laboratory of Separation Science for Analytical Chemistry, Dalian Institute of Chemical Physics, Chinese Academy of Sciences, Dalian, Liaoning 116023, People's Republic of China; University of Chinese Academy of Sciences, Beijing 100049, People's Republic of China*

Jichun Jiang − *CAS Key Laboratory of Separation Science for Analytical Chemistry, Dalian Institute of Chemical Physics, Chinese Academy of Sciences, Dalian, Liaoning 116023, People's Republic of China*

Fan Hu − *Henan Medical Instruments Testing Institute, Zhengzhou 450018, People's Republic of China*

Ping Chen − *CAS Key Laboratory of Separation Science for Analytical Chemistry, Dalian Institute of Chemical Physics, Chinese Academy of Sciences, Dalian, Liaoning 116023, People's Republic of China*

Kaixin Zhu − *State Key Laboratory of Catalysis, iChEM, Dalian Institute of Chemical Physics, Chinese Academy of Sciences, Dalian 116023, China*

Dehui Deng − *State Key Laboratory of Catalysis, iChEM, Dalian Institute of Chemical Physics, Chinese Academy of Sciences, Dalian 116023, China*; orcid.org/0000-0001-9702-0531

Yuanyuan Xie − *CAS Key Laboratory of Separation Science for Analytical Chemistry, Dalian Institute of Chemical*

https://dx.doi.org/10.1021/acs.analchem.0c04081
Anal. Chem. 2021, 93, 2207−2214

Physics, Chinese Academy of Sciences, Dalian, Liaoning 116023, People's Republic of China

Chenxin Wu − *CAS Key Laboratory of Separation Science for Analytical Chemistry, Dalian Institute of Chemical Physics, Chinese Academy of Sciences, Dalian, Liaoning 116023, People's Republic of China; University of Chinese Academy of Sciences, Beijing 100049, People's Republic of China*

Complete contact information is available at: https://pubs.acs.org/10.1021/acs.analchem.0c04081

Author Contributions

The manuscript was written through contributions of all authors. All authors have given approval to the final version of the manuscript.

Notes

The authors declare no competing financial interest.

■ ACKNOWLEDGMENTS

Financial support from the National Natural Science Foundation of China (nos. 21705148, 21904124, and 21927804), the LiaoNing Revitalization Talents Program (XLYC1808022), the Natural Science Foundation of Liaoning Province (2020-MS-017), and the Dalian Institute of Chemical Physics (grants DICP ZZBS201701 and DICP ZZBS201801) is gratefully acknowledged.

■ REFERENCES

(1) Li, Q.; Hua, L.; Xie, Y.; Jiang, J.; Li, H.; Hou, K.; Tian, D.; Li, H. *Analyst* **2019**, *144*, 1104−1109.
(2) Cui, X.; Li, H.; Wang, Y.; Hu, Y.; Hua, L.; Li, H.; Han, X.; Liu, Q.; Yang, F.; He, L.; Chen, X.; Li, Q.; Xiao, J.; Deng, D.; Bao, X. *Chem* **2018**, *4*, 1902−1910.
(3) Xie, Y.; Chen, P.; Hua, L.; Hou, K.; Wang, Y.; Wang, H.; Li, H. *J. Am. Soc. Mass Spectrom.* **2016**, *27*, 144−152.
(4) Jia, L.; Brech, Y. L.; Mauviel, G.; Qi, F.; Frowein, M. B.-v.; Ehlert, S.; Zimmermann, R.; Dufour, A. *Energy Fuels* **2016**, *30*, 1555−1563.
(5) Fischer, M.; Wohlfahrt, S.; Varga, J.; Saraji-bozorgzad, M.; Matuschek, G.; Denner, T.; Zimmermann, R. *J. Therm. Anal.* **2014**, *116*, 1461−1469.
(6) Jiang, J.; Wang, Y.; Hou, K.; Hua, L.; Chen, P.; Liu, W.; Xie, Y.; Li, H. *Anal. Chem.* **2016**, *88*, 5028−5032.
(7) Zhang, P.; Ma, P.; Zhang, H.; Shu, J.; Yang, B.; Li, Z. *Atmos. Environ.* **2017**, *164*, 250−258.
(8) Heide, J.; Czech, H.; Ehlert, S.; Koziorowski, T.; Zimmermann, R. *J. Agric. Food Chem.* **2020**, *68*, 4752−4759.
(9) Toniolo, R.; Pizzariello, A.; Dossi, N.; Lorenzon, S.; Abollino, O.; Bontempelli, G. *Anal. Chem.* **2013**, *85*, 7241−7247.
(10) Wang, Y.; Jiang, J.; Hua, L.; Hou, K.; Xie, Y.; Chen, P.; Liu, W.; Li, Q.; Wang, S.; Li, H. *Anal. Chem.* **2016**, *88*, 9047−9055.
(11) Li, Z.; Xu, C.; Shu, J.; Yang, B.; Zou, Y. *Talanta* **2017**, *165*, 98−106.
(12) Wang, Y.; Hua, L.; Li, Q.; Jiang, J.; Hou, K.; Wu, C.; Li, H. *Anal. Chem.* **2018**, *90*, 5398−5404.
(13) Hanley, L.; Zimmermann, R. *Anal. Chem.* **2009**, *81*, 4174−4182.
(14) Bhardwaj, C.; Hanley, L. *Nat. Prod. Rep.* **2014**, *31*, 756−767.
(15) Adam, T.; Zimmermann, R. *Anal. Bioanal. Chem.* **2007**, *389*, 1941−1951.
(16) Cool, T. A.; Wang, J.; Nakajima, K.; Taatjes, C. A.; Mcllroy, A. *Int. J. Mass Spectrom.* **2005**, *247*, 18−27.
(17) NIST. *National Institute of Standards and Technology (NIST)*; http://webbook.nist.gov/chemistry/ (accessed October 16, 2020).
(18) Eschner, M. S.; Gröger, T. M.; Horvath, T.; Gonin, M.; Zimmermann, R. *Anal. Chem.* **2011**, *83*, 3865−3872.
(19) Mühlberger, F.; Saraji-bozorgzad, M.; Gonin, M.; Fuhrer, K.; Zimmermann, R. *Anal. Chem.* **2007**, *79*, 8118−8124.
(20) Gamez, G.; Zhu, L.; Schmitz, T. A.; Zenobi, R. *Anal. Chem.* **2008**, *80*, 6791−6795.
(21) Hua, L.; Wu, Q.; Hou, K.; Cui, H.; Chen, P.; Wang, W.; Li, J.; Li, H. *Anal. Chem.* **2011**, *83*, 5309−5316.
(22) Xie, Y.; Hua, L.; Hou, K.; Chen, P.; Zhao, W.; Chen, W.; Ju, B.; Li, H. *Anal. Chem.* **2014**, *86*, 7681−7687.
(23) Vadhwana, B.; Belluomo, I.; Boshier, P. R.; Pavlou, C.; Španěl, P.; Hanna, G. B. *Rapid Commun. Mass Spectrom.* **2020**, *34*, No. e8706.
(24) Lacko, M.; Piel, F.; Mauracher, A.; Španěl, P. *Phys. Chem. Chem. Phys.* **2020**, *22*, 10170−10178.
(25) Pedrotti, M.; Khomenko, I.; Fontana, M.; Somenzi, M.; Falchero, L.; Arveda, M.; Cappellin, L.; Fogliano, V.; Biasioli, F. *Int. Dairy J.* **2020**, *109*, 104729.
(26) Yang, B.; Zhang, H.; Shu, J.; Ma, P.; Zhang, P.; Huang, J.; Li, Z.; Xu, C. *Anal. Chem.* **2018**, *90*, 1301−1308.
(27) Zhang, H.; Ma, P.; Shu, J.; Yang, B.; Huang, J. *Anal. Chim. Acta* **2018**, *1035*, 119−128.
(28) Shu, J.; Zou, Y.; Xu, C.; Li, Z.; Sun, W.; Yang, B.; Zhang, H.; Zhang, P.; Ma, P. *Sci. Rep.* **2016**, *6*, 36820.
(29) Huang, J.; Yang, B.; Shu, J.; Zhang, Z.; Li, Z.; Jiang, K. *Anal. Chem.* **2019**, *91*, 5605−5612.
(30) Bohme, D. K.; Mackay, G. I.; Tanner, S. D. *J. Am. Chem. Soc.* **1979**, *101*, 3724−3730.
(31) Racine, A. H.; Payne, A. H.; Remes, P. M.; Glish, G. L. *Anal. Chem.* **2006**, *78*, 4609−4614.
(32) Hua, L.; Hou, K.; Chen, P.; Xie, Y.; Jiang, J.; Wang, Y.; Wang, W.; Li, H. *Anal. Chem.* **2015**, *87*, 2427−2433.
(33) Snyder, D. T.; Fedick, P. W.; Cooks, R. G. *Anal. Chem.* **2016**, *88*, 9572−9581.
(34) Koss, A. R.; Warneke, C.; Yuan, B.; Coggon, M. M.; Veres, P. R.; de Gouw, J. A. *Atmos. Meas. Tech.* **2016**, *9*, 2909−2925.
(35) Hewitt, C. N.; Hayward, S.; Tani, A. *J. Environ. Monit.* **2003**, *5*, 1−7.
(36) Španěl, P.; Žabka, J.; Zymak, I.; Smith, D. *Rapid Commun. Mass Spectrom.* **2017**, *31*, 437−446.
(37) Shestivska, V.; Kolivoška, V.; Kubišta, J.; Smith, D.; Španěl, P. *Rapid Commun. Mass Spectrom.* **2020**, *34*, No. e8744.
(38) Lammert, S. A.; Wells, J. M. *Rapid Commun. Mass Spectrom.* **1996**, *10*, 361−371.
(39) Jiao, F.; Li, J.; Pan, X.; Xiao, J.; Li, H.; Ma, H.; Wei, M.; Pan, Y.; Zhou, Z.; Li, M.; Miao, S.; Zhu, Y.; Xiao, D.; He, T.; Yang, J.; Qi, F.; Fu, Q.; Bao, X. *Science* **2016**, *351*, 1065−1068.
(40) Wang, C.; Chu, Y.; Xu, J.; Wang, Q.; Qi, G.; Gao, P.; Zhou, X.; Deng, F. *Angew. Chem., Int. Ed.* **2018**, *57*, 10197−10201.